ACS APPLIED MATERIALS & INTERFACES

Research Article

www.acsami.org

Glucose Aided Preparation of Tungsten Sulfide/Multi-Wall Carbon Nanotube Hybrid and Use as Counter Electrode in Dye-Sensitized Solar Cells

Jihuai Wu,*[,†] Gentian Yue,[†,‡] Yaoming Xiao,[†,‡] Miaoliang Huang,[†] Jianming Lin,[†] Leqing Fan,[†] Zhang Lan,[†] and Jeng-Yu Lin[‡]

[†]Institute of Material Physical Chemistry, Huaqiao University, Quanzhou 362021, China

[‡]Department of Chemical Engineering, Tatung University, Taipei 104, Taiwan

Supporting Information

ABSTRACT: The tungsten sulfide/multi-wall carbon nanotube (WS_2/MWCNT) hybrid was prepared in the presence of glucose by the hydrothermal route. The hybrid materials were used as counter electrode in the dye-sensitized solar cell (DSSC). The results of cyclic voltammetry measurement and electrochemical impedance spectroscopy indicated that the glucose aided prepared (G-A) WS_2/MWCNT electrode had low charge-transfer resistance (R_{ct}) and high electrocatalytic activity for triiodide reduction. The excellent electrochemical properties for (G-A) WS_2/MWCNT electrode is due to the synergistic effects of WS_2 and MWCNTs, as well as amorphous carbon introduced by glucose. The DSSC based on the G-A WS_2/MWCNT counter electrode achieved a high power conversion efficiency of 7.36%, which is comparable with the performance of the DSSC using Pt counter electrode (7.54%).

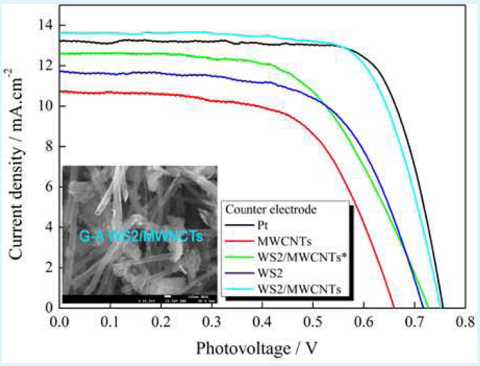

KEYWORDS: *tungsten sulfide, multi-wall carbon nanotubes, counter electrode, dye-sensitized solar cells*

INTRODUCTION

In the past decades, due to the natural resource depletion and environmental issue concerns, the solar energy conversion research has aroused wide attention. Dye-sensitized solar cell (DSSC) is widely considered as an environment-friendly, low-cost, and high power conversion efficient (η) photovoltaic device.[1,2] The DSSC based on traditional platinum (Pt) counter electrode (CE) has achieved a power conversion efficiency of 12%.[3] However, Pt is a noble metal, which increases the cost of the DSSC device. In addition, the atomic Pt can be decomposed to PtI_4 by traditional I^-/I_3^- redox couple, which will affect the device performance, such as long-term stability and so on.[4,5] Thus, it is necessary to develop an economic, stable, effective, and Pt-free CE.

Previous studies have revealed that carbon-based materials,[6,7] conducting polymers,[8,9] sulfides,[10,11] and nitrides[12] possess comparable electrocatalytic activity with Pt metal for the reduction of I_3^- ions. These Pt-free materials are abundant and economic and have a high corrosion resistance property. Among them, multiple-wall carbon nanotubes (MWCNTs) show an eximious potential as an alternative CE due to their large specific surface area, high conductivity, and photochemical stability, as well as good mechanical strength.[13] However, pure MWCNTs do not seem to be an ideal CE material used in DSSC, in view of the limitations of electrocatalytic activity for I_3^- reduction.[14]

Recently, tungsten sulfide (WS_2) was proposed as a potential CE material candidate, which possesses an analogous structure to graphite and graphene, composed of three atom layers: one W layer sandwiched by two S layers, which were stacked by weak vander Waals interactions.[15,16] Li et al.[17] prepared a WS_2 film used as CE in DSSC from commercial WS_2 nanopowders; Wu et al.[18] synthesized WS_2 by a hydrothermal method and introduced it in the DSSC system which showed a power conversion efficiency of 7.73%. Recently, Sudhagar et al.[19] reported the synergistic catalytic effect of cobalt sulfide (CoS) and PEDOT:PSS as CE in DSSC. Li et al.[20] prepared a composite composed of high electrocatalytic TiN nanoparticles and good conductive carbon black and used it as CE for improving photovoltaic performance in DSSC. Das et al.[21] prepared a large CoS-implanted graphene film electrode for DSSCs using the chemical vapor deposition method followed by successive ionic layer absorption and reaction. In the above research, the performance of the DSSC was improved using the sulfide as CE, due to their fast electron-transport network. Thus, it is expected that the performance of the DSSC can be improved using CE materials consisting of transition metal sulfides and MWCNTs.

Received: August 6, 2012
Accepted: November 26, 2012
Published: November 26, 2012

   dx.doi.org/10.1021/am301397e | *ACS Appl. Mater. Interfaces* 2012, 4, 6530−6536

In this paper, a tungsten sulfide/multi-wall carbon nanotube (WS_2/MWCNT) hybrid was prepared in the presence of glucose by a low-temperature hydrothermal method. Using the hybrid as CE material for DSSC, which exhibits a comparable photovoltaic performance to the DSSC based on Pt counter electrode, the results demonstrate the feasibility of glucose aided preparation and provide a novel promising Pt-free counter electrode materials for DSSCs.

EXPERIMENTAL SECTION

Synthesis of WS_2/MWCNTs. Raw MWCNTs (Golden Innovation Business Co.) were refluxed in the 3:1 mixture of 98% H_2SO_4 and 78% HNO_3 at 120 °C for a fixed time to functionalize the graphitic sp^2 carbon into −COOH functional group on the side walls of the MWCNTs. The functionalized MWCNTs were further filtered by suction filtration, washed with deionized water, and then subjected to drying.

The typical synthesis procedure of WS_2/MWCNTs was shown as follows: 1.648 g of sodium tungstate ($Na_2WO_4{\cdot}2H_2O$) (ARCOS, 99%), 1.5224 g of thiourea (ARCOS, 99%), 0.934 g of sodium borohydride (ARCOS, 99%), and 0.6 g of glucose (ARCOS, 99%) were put into a Teflon-lined stainless steel autoclave with capacity of 150 mL; 70 mL of pyridine (ARCOS, 99%) and 0.748 g of Aliquat-336 (ARCOS, 99%) were added to fill the autoclave to 50% of its total volume. After that, a predetermined amount of MWCNTs (Golden Innovation Business Co.) were added; the mixture was sonicated for 30 min. The autoclave was tightly sealed and maintained at 200 °C for 48 h without intentional control of ramping or cooling rate; the product of black precipitate was collected by filter and washed with ethanol and distilled water for at least 5 times and then dried in a vacuum oven at 100 °C for 24 h. Thus, the WS_2/MWCNTs were obtained. For comparison, the sample without glucose aided growth also was synthesized and was designated as WS_2/MWCNTs*.

Preparation of Counter Electrode. Firstly, the fluorine-doped tin oxide transparent (FTO) glass substrate (8 Ω·cm^{-2}, Hartford Glass Co., USA) was cut into 1 × 2 cm^2 carefully and bore a hole on the conductive side for injecting liquid electrolyte. After that, the FTO was ultrasonically cleaned sequentially in detergent, acetone, and distilled water for 10 min, in sequence, and the FTO was stored in isopropyl alcohol (IPA, ECHO Chemicals). The CE was prepared by a slurry coating procedure. The slurry was obtained by dissolving 80 wt % of the synthesized WS_2/MWCNTs, 10 wt % of acetylene black, and 10 wt % of polyvinylidene fluoride grinded in *N*-methyl-2-pyrrolidinone and then was stirred for 12 h. Subsequently, the as-prepared slurry was coated on the FTO substrates with different thicknesses using the doctor blade method and dried at 100 °C for 24 h in a vacuum oven. Thus, the CEs were obtained.

Fabrication of DSSC. The TiO_2 anode was prepared as described previously.[22,23] In brief, a thin TiO_2 blocking layer was deposited on the FTO substrate with drilling by immersing the FTO in the 0.15 M $TiCl_4$ isopropanol solution for 12 h, followed by sintering at 450 °C for 30 min in air. Subsequently, the TiO_2 layer with particle size of 10−20 nm was coated onto the blocking layer using the doctor blade method and then sintered at 450 °C for 30 min in air. The dye was loaded by immersing the TiO_2 anode in the 0.3 mM dye N719 ethanol solution for 24 h. Thus, the dye-sensitized TiO_2 anode with thickness of 6−8 μm was obtained. The DSSC (shown in Figure 1) was fabricated by injecting the liquid electrolyte (0.05 M I_2, 0.1 M LiI, 0.6 M tetrabutylammonium iodide, and 0.5 M TBP in acetonitrile) in the aperture between the dye-sensitized TiO_2 electrode and the CE. The two electrodes were clipped together and wrapped with thermoplastic hot-melt Surlyn.

Characterization and Measurement. The micromorphologies and energy dispersive spectroscopy (EDS) of the samples were characterized using a JSM-7600F field emission scanning electron microscope (SEM). Fourier transforms infrared (FT-IR) spectroscopy measurement was carried out using a Nicolet Impact 410 FT-IR spectrometer. The specific surface area Brunauer−Emmett−Teller (BET) was measured using a JW-K analyzer by nitrogen absorption.

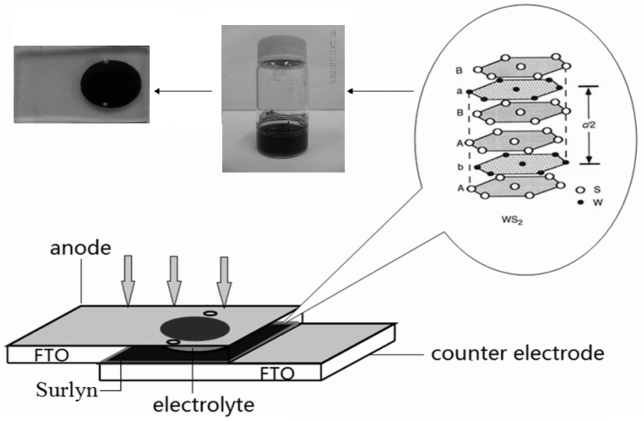

Figure 1. Schematic diagram of the DSSC with WS_2/MWCNT counter electrode.

The ultraviolet-visible (UV-vis) absorption spectrum of sample was measured using an Optizen (3100UV) spectrophotometer. The compositions of samples were analyzed by glancing incident X-ray diffractometer (GIXRD6000, Shimadzu Corporation, Japan). Cyclic voltammetry measurements (CV) were conducted, in which an as-prepared CE was taken as the working electrode in a three-electrode one-compartment cell, one 4 cm^2 of Pt sheet auxiliary electrode, and one Pt wire reference electrode in the acetonitrile solution consisting of 10 mM LiI, 1 mM I_2, and 0.1 M $LiClO_4$. The electrochemical impedance spectroscopy (EIS) measurement was carried out with two identical electrodes sealed with a thermoplastic hot-melt Surlyn and leaving an exposed area of 0.64 cm^2. The electrolyte used in the device tests was also injected into the EIS symmetric cells. The EIS tests were carried out simulating open-circuit conditions at ambient atmosphere using a CHI660D (CHI660D, Shanghai Chenhua Device Company, China) electrochemical measurement system at a constant temperature of 20 °C with AC signal amplitude of 20 mV in the frequency range from 0.1 to 10^5 Hz at 0 V DC bias in the dark. The complex nonlinear least square analysis of the Nyquist plots were made with the ZSimdemo version 3.30d.

The photovoltaic parameters of the DSSC were determined by measuring photocurrent−photovoltage (J−V) characteristic curves under a white light irradiation of 100 mW·cm^{-2} (AM 1.5) from a solar simulator (XQ-500W, Shanghai Photoelectricity Device Company, China) in ambient atmosphere. The fill factor (FF) and the power conversion efficiency (η) of the DSSC were calculated according to the following equations:[24]

$$\eta\ (\%) = \frac{V_{max} \times J_{max}}{P_{in}} \times 100\% = \frac{V_{OC} \times J_{SC} \times FF}{P_{in}} \times 100\% \quad (1)$$

$$FF = \frac{V_{max} \times J_{max}}{V_{OC} \times J_{SC}} \quad (2)$$

where J_{SC} is the short-circuit current density (mA·cm^{-2}), V_{OC} is the open-circuit voltage (V), P_{in} is the incident light power, and J_{max} (mA·cm^{-2}) and V_{max} (V) are the current density and voltage at the point of maximum power output in the J−V curve, respectively.

RESULTS AND DISCUSSION

Morphology and Composition. Figure 2 presents the SEM images of WS_2, MWCNTs, and WS_2/MWCNTs. As shown in Figure 2a, the WS_2 possesses graphene-like lamellar structure, providing a large specific surface area. Figure 2b exhibits the crude morphologies of the MWCNTs with fiber-like structure, which possess a large specific surface area. From the Figure 2c,d, it is observed that the WS_2 has been successfully grown on the surface of MWCNTs. The specific

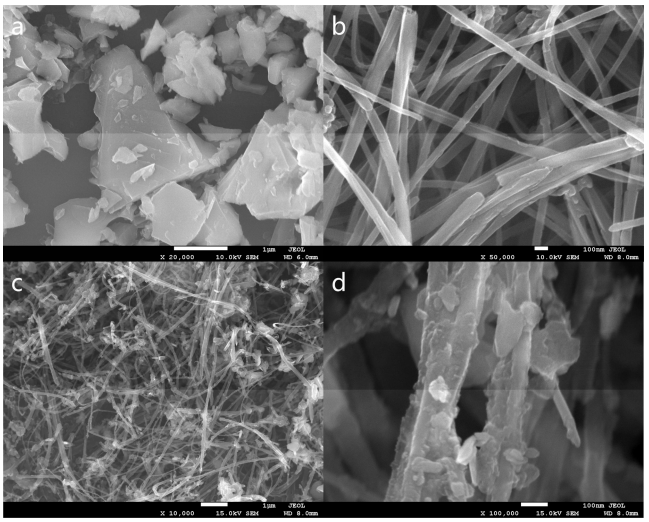

Figure 2. SEM images of (a) WS_2, (b) MWCNTs, and (c and d) WS_2/MWCNTs.

surface area of WS_2/MWCNTs is calculated as about 230 $m^2 \cdot g^{-1}$ by BET method according to N_2 absorption−desorption isotherms of WS_2/MWCNTs shown in Figure S1, Supporting Information. The large specific surface area favors the improvement of electrochemical activity and the photovoltaic performance of DSSC.

The EDS spectrum of the WS_2/MWCNTs was characterized and shown in Figure S2, Supporting Information. The elements of C, O, S, and W are found in the sample, where the elements of C, W, and S show strong signals, which indicate the formation of WS_2/MWCNTs.

Figure 3 shows the X-ray diffraction (XRD) patterns of MWCNTs, WS_2* (without glucose aided growth), WS_2 (with glucose aided growth), and WS_2/MWCNTs. The diffraction peaks in the curve a can be indexed to MWCNTs hexagonal C (JCPDS Card No.75-1621) with its (002) plane at 26.29° and (200) plane at 43.12°,[25] marked as ☆. All the peaks in the curve b can be indexed to the hexagonal WS_2 (JCPDS card No. 08-0237) with its (002), (100), and (110) planes at 14.30°, 32.39°, and 56.47°,[26] marked as ★, respectively. The strongest peak of 14.30° can be identified as the presence of well-stacked layered structure.[21] Compared to the WS_2* without glucose aided growth (curve b), the WS_2 with glucose aided growth (curve c) has a strong peak at 26.29°, which is the signal of MWCNT and carbon. The peak is further enhanced in the curve d, which is due to the synergistic effect of carbon and MWCNTs in WS_2/MWCNTs.[27] It indicates that the glucose is transferred into carbon (some amorphous carbon can not be observed from the XRD) during the hydrothermal process at 200 °C for 48 h. The XRD pattern of the WS_2/MWCNTs exhibits characteristic peaks of MWCNTs, carbon, and WS_2, indicating that WS_2/MWCNTs in the presence of glucose was prepared successfully.

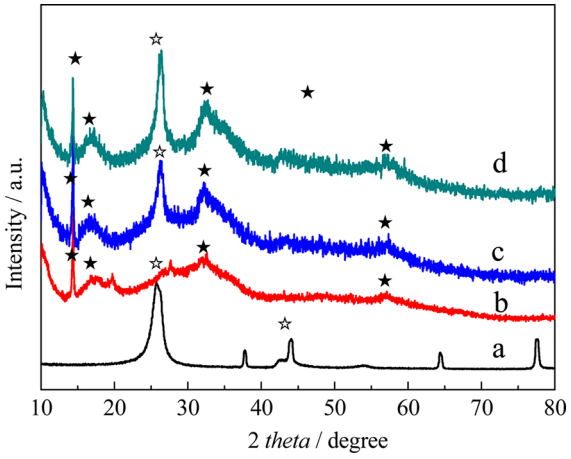

Figure 3. XRD patterns of (a) MWCNTs, (b) WS_2*, (c) WS_2, and (d) WS_2/MWCNTs.

Figure 4 shows the FT-IR spectra of MWCNTs, WS_2, WS_2/MWCNTs*, and WS_2/MWCNTs, respectively. As shown in the curve a, the absorption bands at 1573 cm^{-1} are associated with the C═C stretching of the aromatic groups.[28] The peaks at around 1211, 1706, and 1376 cm^{-1} are due to the C═O stretching vibrations and hydroxyl groups (−OH) bending deformation of the carboxylic groups (−COOH) from the acid-oxidized MWCNT surface.[29] Four bands appearing at 880, 1610, 2068, and 2918 cm^{-1} in the curve b can be attributed to the W−S stretching vibrations and bending vibrations. Most of the characteristic bands associated with MWCNTs, carbon, and WS_2 are observed in the curves c and d with a slight shift in position for WS_2/MWCNTs* and WS_2/MWCNTs. The band related with C═C stretching of the aromatic groups is observed at 1573 cm^{-1}. The 2068 and 2918 cm^{-1} bands in the WS_2, assigned to W−S, are clearly observed in the samples.

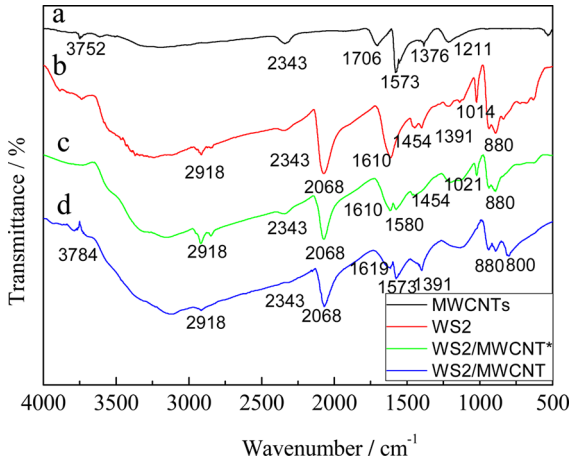

Figure 4. FT-IR of (a) MWCNTs; (b) WS_2; (c) WS_2/MWCNTs*; (d) WS_2/MWCNTs.

Cyclic Voltammetry Analysis. Figure 5a shows the CV curves for the Pt, WS_2, MWCNT, WS_2/MWCNT*, and WS_2/MWCNT electrodes as working electrodes in I^-/I_3^- redox electrolyte. The peaks in the positive side is known as the oxidation peak, and the negative one is the reduction peak. The reaction at the interface of the electrode and the electrolyte for DSSC is represented as follows:[30]

$$3I^- \rightarrow I_3^- + 2e^- \text{ (oxidation)} \quad (3)$$

$$I_3^- + 2e^- \rightarrow 3I^- \text{ (reduction)} \quad (4)$$

The cathodic peak potentials of the WS_2 and WS_2/MWCNT electrodes are −0.14 and −0.13 V, respectively, indicating that the introduction of MWCNTs improves the electrocatalytic activity of the electrode and decreases overpotential for reduction of I_3^- to I^-. The cathodic peak potentials of the

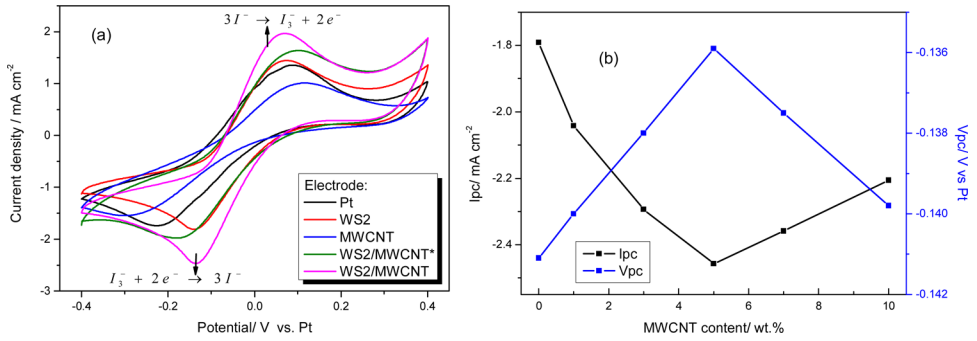

Figure 5. (a) CVs of the Pt, WS_2, MWCNT, WS_2/MWCNT*, and WS_2/MWCNT electrodes at a scan rate of 10 mV·s^{-1} in the I_3^-/I^- redox electrolytes; (b) the relationship between the MWCNT content in the hybrid vs. the cathodic peak current density (I_{pc}) and potential (V_{pc}) for the WS_2/MWCNT CEs.

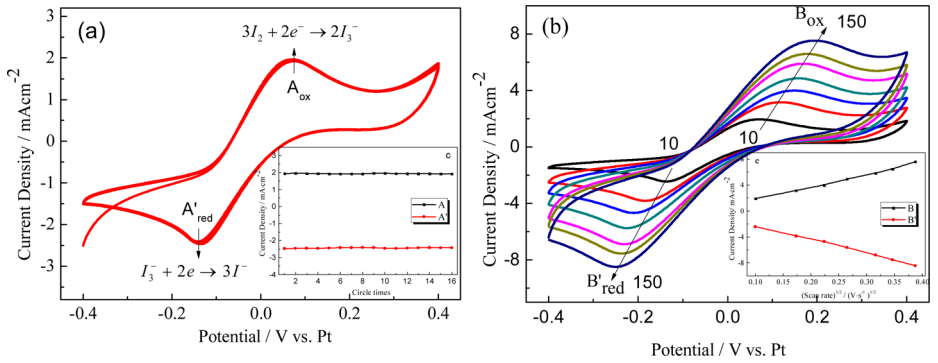

Figure 6. (a) 16 times continuous cycle scans CVs of the WS_2/MWCNT electrode with the scan rate of 10 mV·s^{-1}; inset figure is the relationship between the cycles and the maximum redox peak currents. (b) CVs for the WS_2/MWCNT electrode with different scan rates (from inner to outer: 10, 30, 50, ..., 150 mV·s^{-1}); inset figure is the redox peaks current versus square root of scan rate.

WS_2/MWCNT* and WS_2/MWCNT electrodes are −0.17 and −0.13 V, respectively. The smaller cathodic peak potential for WS_2/MWCNTs than that of WS_2/MWCNTs* is due to the large specific surface area offering by the amorphous carbon resulting from the glucose aided preparation. On the other hand, the peak current densities of the glucose aided grown WS_2/MWCNT, WS_2/MWCNT*, WS_2, MWCNT, and Pt electrodes are −2.46, −1.97, −1.81, −1.54, and −1.74 mA·cm^{-2}, respectively. It means that the cooperation between MWCNTs and WS_2 can enhance the conductivity of the hybrid, and the glucose aided preparation can further improve the conductivity of the electrode. In addition, the MWCNT electrode shows the smallest cathodic peak potential and current density, which implies that the MWCNTs have poor conductivity and catalytic activity.

CVs of WS_2/MWCNT electrodes with different MWCNT contents were measured and shown in the Figure S3, Supporting Information; according to the figure, the relationships between the MWCNT contents in the hybrid electrode vs. the cathodic peak current density current (I_{pc}) and potential (V_{pc}) are extracted and shown in Figure 5b. It can be seen that, with increasing the MWCNT percentage in the electrode from 0 to 5 wt %, the I_{pc} absolute values increase and V_{pc} absolute values decrease. While beyond the 5 wt %, with the increases of the MWCNT percentage, the I_{pc} absolute values decrease and V_{pc} absolute increases. It is known that the CV behavior mainly depends on the catalytic activity and conductivity of electrode materials. The higher conductive electrode produces larger I_{pc}, and the better catalytic electrode has lower overpotential and smaller V_{pc}. Owing to the synergistic effect between MWCNT and WS_2, with the increase of the MWCNT percentage, the I_{pc} absolute values increase and the V_{pc} absolute values decrease firstly. In our experiment conditions, the electrode containing MWCNTs 5 wt % achieves a highest I_{pc} absolute value of 2.46 mA·cm^{-2} and lowest V_{pc} absolute value of 0.13 V, respectively. However, when the amount of MWCNTs exceeds 5 wt %, owing to poor conductivity and catalytic activity for MWCNTs, the I_{pc} absolute values decrease and the V_{pc} absolute values increase with the increase of the MWCNT percentage further.

Figure 6a shows the 16 times continuous CV curves for the WS_2/MWCNT electrode in the I_3^-/I^- system at the scan rate of 10 mV·s^{-1}. The curves have not changed after the consecutive 16 cycles, and there is good linear relationship between both redox peak currents and the cycle times shown in the figure inset. This means that the WS_2/MWCNT film not only possesses excellent electrochemical stability, but it is also attached firmly and uniformly on the FTO substrate.[8] Figure 6b shows CVs for WS_2/MWCNT electrode with different scan rates. The cathodic and anodic peak current densities regularly shifted to the negative and positive directions with increasing scan rate. Also, there is a good linear relationship between the square root of the scan rate and current density shown in the figure inset. This phenomenon demonstrates that the charge transferring in the electrolyte/electrode interface is a diffusion limitation process, indicating no specific interaction between I^-/I_3^- redox couple and WS_2/MWCNT electrode like the Pt electrode.[31]

Electrochemical Impedance Analysis. To evaluate the influence of MWCNTs on the performance of electrode, the EIS measurement was carried out with a dummy cell assembled

by two identical samples as shown in Figure 7. The EIS data was obtained by fitting the Nyquist plots with an equivalent

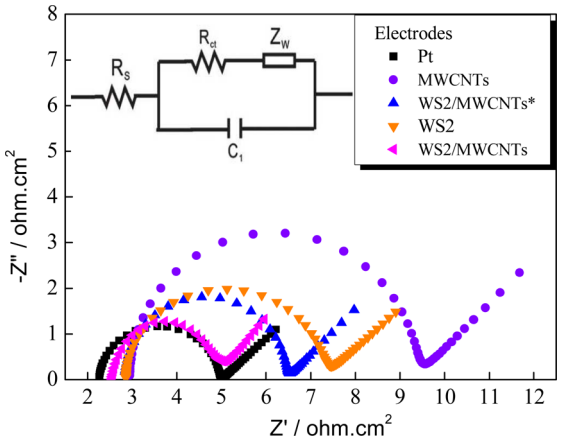

Figure 7. Nyquist plots of symmetrical Pt, MWCNT, WS_2/MWCNT*, WS_2, and WS_2/MWCNT electrodes; the equivalent circuit is shown in the inset, including a component R_s = serial resistance; R_{ct} = charge-transfer resistance of single electrode; C_1 = double layer capacitance; Z_W = diffusion impedance.

circuit diagram (shown in the inset of Figure 7), in which R_{ct} is the charge-transfer resistance in the electrolyte/electrode interface for I_3^-/I^- redox reaction, R_s is the series resistance of electrode, and C_1 represents the double layer capacitance,[32,33] and the fitting parameters are listed in Table 1. Additionally, the exchange current density (J_0) is calculated from the eq 5 for different dummy cells.[34]

$$J_0 = \frac{RT}{nFR_{ct}} \quad (5)$$

where R is the gas constant, T is the temperature (298 k), F was Faraday's constant, and n (n = 2) is the number of electrons involved in the reduction of I_3^- at the electrode.

As presented as in Figure 7 and Table 1, the R_s for the Pt, MWCNT, WS_2, WS_2/MWCNT*, and WS_2/MWCNT electrodes are 2.27, 2.95, 2.86, 2.85, and 2.54 Ω·cm^2, respectively. The R_{ct} for the Pt, MWCNT, WS_2, WS_2/MWCNT*, and WS_2/MWCNT electrodes are 2.74, 6.60, 4.60, 3.47, and 2.49 Ω·cm^2, respectively. The R_s and R_{ct} of the WS_2/MWCNT electrode smaller than those of the WS_2/MWCNT* electrode can be attributed to the larger specific surface area for WS_2/MWCNTs offered by the amorphous carbon originated from glucose aided preparation. The R_{ct} and R_s of the WS_2/MWCNTs are 2.49 and 2.54 Ω·cm^2, which are smaller than that of WS_2 (4.60 and 2.86 Ω·cm^2). This means that the synergistic effect between MWCNTs and WS_2 can increase the conductivity of the hybrid. It is significant that the WS_2/MWCNT electrode has similar R_{ct} and R_s with Pt electrode.

To investigate the influence of the MWCNTs on the impedance of the electrodes, the EIS curves for the electrodes with different MWCNT contents were measured and shown in Figure S4 and Table S1, Supporting Information. The R_{ct} values decrease gradually with the increase in MWCNT percentage from 0 to 5 wt %. When the MWCNT amount is 5 wt %, the electrode obtains the smallest R_{ct} of 2.49 Ω·cm^2, and the highest exchange current density (J_0) of 5.16 mA·cm^{-2}. With the further increase of MWCNT amount in the electrode, the R_s and R_{ct} increase, and J_0 decreases. It is known that the impedance behavior for electrode in I_3^-/I^- electrolyte mainly depends on the catalytic activity and conductivity of electrode materials. The higher conductive and catalytic electrode produces smaller impedance. Owing to the synergistic effect between MWCNT and WS_2, with the increase of the MWCNT percentage, the R_{ct} and R_s values decrease first. However, when the MWCNT amount exceeds 5 wt %, owing to poor conductivity and catalytic activity for MWCNTs, the R_{ct} and R_s values increase with the increase of the MWCNT percentage further. These results are accorded with the CV measurements.

Photovoltaic Performance of DSSCs. The incident photon-to-current efficiency (IPCE) of the DSSCs with Pt and WS_2/MWCNT (5 wt %) CEs are shown in Figure 8. It is

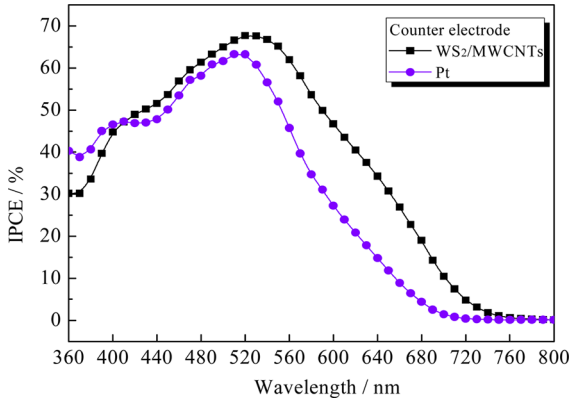

Figure 8. IPCE spectra of the DSSCs with Pt and the WS_2/MWCNT (5 wt %) counter electrodes.

observed that the IPCE curves of the DSSCs using the Pt and WS_2/MWCNT CEs both have good photoelectric responses in the 360−700 nm spectral range. It is noticeable that the DSSC based on WS_2/MWCNT CE exhibits a higher IPCE value (67.7%) than that of the DSSC based on Pt CE (63.8%) in the wavelength range of 410−700 nm. One reason for the phenomenon is that the WS_2/MWCNT film has smaller transmission from 320 to 800 nm (Figure S6, Supporting Information) than the the Pt film does; it means that more incident light is harvested by the WS_2/MWCNT film.

Table 1. EIS Parameters of the Dummy Cells and Photovoltaic Performance of the DSSCs with the Same Electrodes

electrodes	R_s (Ω·cm^2)	R_{ct} (Ω·cm^2)	J_0 (mA·cm^{-2})	V_{oc} (V)	J_{SC} (mA·cm^{-2})	FF	η (%)
Pt	2.27 ± 0.01	2.74 ± 0.01	4.69	0.76	13.23	0.75	7.54
WS_2	2.86 ± 0.01	4.60 ± 0.01	2.79	0.72	11.72	0.63	5.32
MWCNTs	2.95 ± 0.01	6.60 ± 0.01	1.95	0.66	10.77	0.61	4.34
WS_2/MWCNT*[a]	2.85 ± 0.01	3.47 ± 0.01	3.70	0.73	12.65	0.59	5.45
WS_2/MWCNT[a]	2.54 ± 0.01	2.49 ± 0.01	5.16	0.75	13.63	0.72	7.36

[a]The MWCNT content is 5 wt %.

dx.doi.org/10.1021/am301397e | ACS Appl. Mater. Interfaces 2012, 4, 6530−6536

Figure 9 shows the $J-V$ curves of DSSCs based on different counter electrodes under a simulated solar irradiation of 100 mW·cm^{-2} (AM 1.5), and the photovoltaic parameters are listed in Table 1. The power conversion efficiencies of DSSCs based on Pt, MWCNT, WS_2, WS_2/MWCNT*, and WS_2/MWCNT CEs are 7.54%, 4.34%, 5.32%, 5.45%, and 7.36%, respectively. The DSSCs with and without glucose aided preparation show a large difference in the FF, which can be contributing to the large specific surface area offering by the amorphous carbon resulting from the glucose. The higher J_{SC} for the DSSC with WS_2/MWCNT CE than that for the DSSC with Pt CE mainly is due to higher IPCE value for the former than the latter in the wavelength range of 410−700 nm. However, in ultraviolet range (less 400 nm), higher IPCE value for the Pt CE than that of the WS_2/MWCNT CE compensates partly the J_{SC} difference between the two DSSCs.

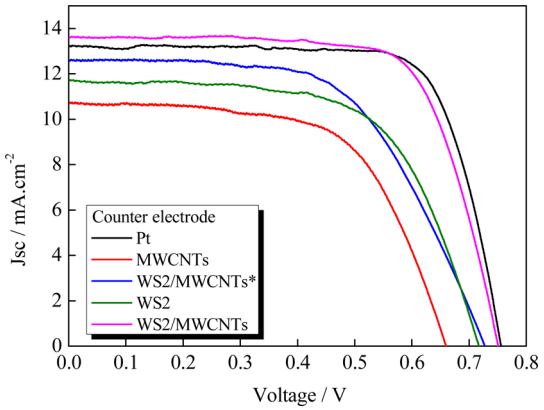

Figure 9. Photocurrent−voltage curves of the DSSCs with Pt, MWCNT, WS_2, WS_2/MWCNT*, and WS_2/MWCNT CEs under a simulated solar irradiation of 100 mW·cm^{-2}.

Figure S5 and Table S1, Supporting Information, show the η values of the DSSCs based on the WS_2/MWCNT CEs with different MWCNT amounts. With the increase of MWCNT amount in the WS_2/MWCNT hybrid CEs, the J_{SC} value increases from 1.72 to 13.63 mA·cm^{-2} and then decreases with further increasing MWCNT amount. When the MWCNT amount is 5 wt %, the DSSC obtained the best photovoltaic performance including J_{SC} of 13.63 mA·cm^{-2}, FF of 0.72, V_{oc} of 0.75, and an extraordinary high η of 7.36%, while the η value for the DSSC with conventional Pt CE is 7.54%. This is mainly because the glucose aided prepared WS_2/MWCNT (5 wt %) electrode has large specific surface area, lower charge-transfer resistance, and good electrocatalytic activity for reduction of iodine.[35] In addition, the WS_2/MWCNT (5 wt %) film shows the smaller transmission from 320 to 800 nm (Figure S6, Supporting Information) than the Pt film does, it means that more incident light is harvested by the WS_2/MWCNT film, which is helpful for improving J_{SC} for the DSSCs.

CONCLUSIONS

The tungsten sulfide/multi-wall carbon nanotube (WS_2/MWCNT) hybrid was successfully prepared in the presence of glucose by the hydrothermal method. The hybrid film was used as Pt-free counter electrode in dye-sensitized solar cells. The characterization of SEM, BET, XRD, FTIR, CV, and EIS indicated that the glucose aided prepared (G-A) WS_2/MWCNT electrode had large surface area, low charge-transfer resistance (R_{ct}), and high electrocatalytic activity for triiodide reduction. These excellent electrochemical properties for G-A WS_2/MWCNT electrode come from the synergistic effects of WS_2 and MWCNTs, as well as amorphous carbon introduced by glucose. Under an optimal condition, the DSSC based on the G-A WS_2/MWCNT counter electrode achieved a power conversion efficiency of 7.36% under a simulated solar irradiation of 100 mW·cm^{-2}, which is comparable with the performance of the DSSC based on Pt counter electrode (7.54%). These results indicate that the G-A WS_2/MWCNTs is a promising CE material and provides a novel way for the use of low-cost transition metal sulfides as CE in DSSCs.

ASSOCIATED CONTENT

Supporting Information

Figures S1−S6 and Table S1, in detail: Figure S1, N_2 absorption−desorption isotherms of WS_2/MWCNTs; Figure S2, EDS spectrum of the WS_2/MWCNTs; Figure S3, CVs of WS_2/MWCNT electrodes with different MWCNT contents; Figure S4, EIS spectra of WS_2/MWCNT electrodes with different MWCNT contents; Figure S5, $J-V$ curves for the DSSCs with WS_2/MWCNT electrode in different MWCNT contents; Figure S6, UV-vis reflection and transmission spectra for Pt and WS_2/MWCNT electrodes; Table S1, EIS data of WS_2/MWCNT electrodes with different MWCNT contents and photovoltaic data of corresponding DSSCs. This material is available free of charge via the Internet at http://pubs.acs.org.

AUTHOR INFORMATION

Corresponding Author

*Tel.: +86 595 22693899. Fax: +86 595 22692229. E-mail: jhwu@hqu.edu.cn.

Notes

The authors declare no competing financial interest.

ACKNOWLEDGMENTS

The authors express heartfelt thanks for joint support by the National High Technology Research and Development Program of China (No. 2009AA03Z217), the National Natural Science Foundation of China (No. U1205112, No. 90922028, and No. 211204), and the Science Council in Taiwan (No. NSC-100-2221-E-036-022).

REFERENCES

(1) O'Regan, B.; Gratzel, M. *Nature* **1991**, *353*, 737−740.
(2) Gratzel, M. *Nature* **2001**, *414*, 338−344.
(3) Yella, A.; Lee, H. W.; Tsao, H. N.; Yi, C. Y.; Chandiran, A. K.; Nazeeruddin, M. K.; Diau, E. W. G.; Yeh, C. Y.; Zakeeruddin, S. M.; Gratzel, M. *Science* **2011**, *334*, 629−634.
(4) Olsen, E.; Hagen, G.; Lindquist, S.E. *Sol. Energy Mater. Sol. Cells* **2000**, *63*, 267−273.
(5) Kay, A.; Gratzel, M. *Sol. Energy Mater. Sol. Cells* **1996**, *44*, 99−117.
(6) Hino, T.; Ogawa, Y.; Kuramoto, N. *Carbon* **2006**, *44*, 880−887.
(7) Choi, H.; Kim, H.; Hwang, S.; Choi, W.; Jeon, M. *Sol. Energy Mater. Sol. Cells* **2011**, *95*, 323−325.
(8) Li, Q.; Wu, J.; Tang, Q.; Lan, Z.; Li, P.; Lin, J. *Electrochem. Commun.* **2008**, *10*, 1299−1302.
(9) Sun, H.; Luo, Y.; Zhang, Y.; Li, D.; Yu, Z.; Li, K.; Meng, Q. *J. Phys. Chem. C* **2010**, *114*, 11673−11679.
(10) Wang, M. K.; Anghel, A. M.; Marsan, B.; Ha, N. C.; Pootrakulchote, N.; Zakeeruddin, S. M.; Gratzel, M. *J. Am. Chem. Soc.* **2009**, *131*, 15976−15977.

(11) Sun, H. C.; Qin, D.; Huang, S. Q.; Guo, X. Z.; Li, D. M.; Luo, Y. H.; Meng, Q. B. *Energy Environ. Sci.* **2011**, *4*, 2630−2637.
(12) Li, G. R.; Song, J.; Pan, G. L.; Gao, X. P. *Energy Environ. Sci.* **2011**, *4*, 1680−1683.
(13) Nugent, J. M.; Santhanam, K. S. V.; Rubio, A.; Ajayan, P. M. *Nano Lett.* **2001**, *1*, 87−91.
(14) Lin, J.; Lien, C.; Chou, S. *J. Solid State Electrochem.* **2012**, *16*, 1415−1421.
(15) Tenne, R.; Margulis, L.; Genut, M.; Hodes, G. *Nature* **1992**, *360*, 444−446.
(16) Li, Y. F.; Zhou, Z.; Zhang, S. B.; Chen, Z. F. *J. Am. Chem. Soc.* **2008**, *130*, 16739−16744.
(17) Li, S. J.; Chen, Z.; Zhang, W. F. *Mater. Lett.* **2012**, *72*, 22−24.
(18) Wu, M. X.; Wang, Y. D.; Lin, X.; Yu, N. S.; Wang, L.; Wang, L. L.; Hagfeldt, A.; Ma, T. L. *Phys. Chem. Chem. Phys.* **2011**, *13*, 19298−19301.
(19) Sudhagar, P.; Nagarajan, S.; Lee, Y.; Song, D.; Son, T.; Cho, W.; Heo, M.; Lee, K.; Won, J.; Kang, Y. *ACS Appl. Mater. Interfaces* **2011**, *3*, 1838−1843.
(20) Li, G.; Wang, F.; Song, J.; Xiong, F.; Gao, X. *Electrochim. Acta* **2012**, *65*, 216−220.
(21) Das, S.; Sudhagar, P.; Nagarajan, S.; Ito, E.; Lee, S.; Kang, Y.; Choi, W. *Carbon* **2012**, *50*, 4815−4821.
(22) Wu, J.; Hao, S.; Lan, Z.; Lin, J.; Huang, M.; Huang, Y.; Sato, T.; Yin, S. *Adv. Funct. Mater.* **2007**, *17*, 2645−2652.
(23) Wu, J.; Lan, Z.; Lin, J.; Huang, M.; Hao, S.; Sato, T.; Yin, S. *Adv. Mater.* **2007**, *19*, 4006−4011.
(24) Hagfeldt, A.; Boschloo, G.; Sun, L.; Kloo, L.; Pettersson, H. *Chem. Rev.* **2010**, *110*, 6595−6663.
(25) He, H.; Gao, C. *Molecules* **2010**, *15*, 4679−4694.
(26) Panigrahi, P. K.; Pathak, A. *Sci. Technol. Adv. Mater.* **2008**, *9*, 045008.
(27) Ding, K. Q.; Yang, G. K. *Electrochim. Acta* **2010**, *55*, 2319−2324.
(28) Hsin, Y. L.; Lai, J. Y.; Hwang, K. C.; Lo, S. C.; Chen, F. R.; Kai, J. J. *Carbon* **2006**, *44*, 3328−3335.
(29) Wu, T. M.; Lin, Y. W.; Liao, C. S. *Carbon* **2005**, *43*, 734−740.
(30) Veerappan, G.; Kwon, W.; Rhee, S. *J. Power Sources* **2011**, *196*, 10798−10805.
(31) Hauch, A.; Georg, A. *Electrochim. Acta* **2001**, *46*, 3457−3466.
(32) Mei, X.; Cho, S.; Fan, B.; Quyang, J. *Nanotechnology* **2010**, 21395202.
(33) Li, G. R.; Wang, F.; Jiang, Q.W.; Gao, X. P.; Shen, P. W. *Angew. Chem., Int. Ed.* **2010**, *49*, 3653−3656.
(34) Wu, M. X.; Lin, X.; Wang, T. H.; Qiu, J. H.; Ma, T. L. *Energy Environ. Sci.* **2011**, *4*, 2308−2315.
(35) Joshi, P.; Xie, Y.; Ropp, M.; Galipeau, D.; Bailey, S.; Qiao, Q. *Energy Environ. Sci.* **2009**, *2*, 426−429.